Molecular Biology of the Cell
Vol. 15, 2470–2483, May 2004

Cytoplasmic Dynein–Dynactin Complex Is Required for Spermatid Growth but Not Axoneme Assembly in *Drosophila*[V]

Anindya Ghosh-Roy, Madhura Kulkarni, Vikash Kumar, Seema Shirolikar, and Krishanu Ray*

Tata Institute of Fundamental Research, Mumbai 400 005, India

Submitted November 26, 2003; Revised February 18, 2004; Accepted February 25, 2004
Monitoring Editor: Jennifer Lippincott-Schwartz

Spermatids derived from a single gonial cell remain interconnected within a cyst and elongate by synchronized growth inside the testis in *Drosophila*. Cylindrical spectrin-rich elongation cones form at their distal ends during the growth. The mechanism underlying this process is poorly understood. We found that developing sperm tails were abnormally coiled at the growing ends inside the cysts in the *Drosophila* Dynein light chain 1 (*ddlc1*) hemizygous mutant testis. A quantitative assay showed that average number of elongation cones was reduced, they were increasingly deformed, and average cyst lengths were shortened in *ddlc1* hemizygous testes. These phenotypes were further enhanced by additional partial reduction of *Dhc64C* and *Glued* and rescued by Myc-PIN/LC8 expression in the gonial cells in *ddlc1* backgrounds. Furthermore, DDLC1, DHC, and GLUED were enriched at the distal ends of growing spermatids. Finally, ultrastructure analysis of *ddlc1* testes revealed abnormally formed interspermatid membrane, but the 9 + 2 microtubule organization, the radial spoke structures, and the Dynein arms of the axoneme were normal. Together, these findings suggest that axoneme assembly and spermatid growth involve independent mechanisms in *Drosophila* and DDLC1 interacts with the Dynein–Dynactin complex at the distal ends of spermatids to maintain the spectrin cytoskeleton assembly and cell growth.

INTRODUCTION

Spermatogenesis is a complex cell differentiation process that involves both mitotic and meiotic cell divisions followed by dramatic cytoskeletal reorganizations and cell growth. In *Drosophila*, for example, an undifferentiated gonial cell produces 64 nearly spherical spermatocytes after four rounds of mitosis and a meiosis and then all of them simultaneously grow to form ~1.8-mm-long spermatids (Lindsley and Tokuyasu, 1980; Fuller, 1993). Axoneme growth inside each spermatid is synchronized with the cell growth and thus it always fits the length of the spermatid as it grows. Once fully grown, the spermatids inside a cyst are individualized to form motile sperm, which then swim into the seminal vesicle. The mechanism of sperm individualization is understood to some extent (Arama *et al*., 2003; Noguchi and Miller, 2003). However, the mechanism involved in spermatid growth remained unclear.

Intraflagellar transport (IFT) plays an important role in the growth of flagella in unicellular organisms such as *Chlamydomonas* and in the primary cilia of various other organisms (Rosenbaum and Witman, 2002). Mutations affecting the IFT reduce the length of the flagella/cilia as well as the axoneme (Kozminski *et al*., 1995; Pazour *et al*., 1998; Signor *et al*., 1999; Qin *et al*., 2001), and a recent study has shown that the components of the radial spoke structure of the axoneme is transported in and out of the flagella by the IFT (Qin *et al*., 2004). Thus, axoneme growth is intimately linked to that of flagella and cilia. Although the molecular mechanism of flagella formation in mammalian sperm is not so clearly defined, a recent report indicated that the IFT mechanism could also control the formation of sperm tails in mammalian testes (Taulman *et al*., 2001). Recent studies in *Drosophila*, however, have shown that Kinesin II-dependent anterograde IFT is not required to grow the flagella of spermatids (Han *et al*., 2003; Sarpal *et al*., 2003), and studies with rnRacGAP mutants suggested that the Ras/Rac-mediated cytoskeletal reorganization would play an important role in spermatid growth (Bergeret *et al*., 2001). Therefore, spermatids in *Drosophila* seem to grow their tails by using a distinctly different mechanism, which could be similar to that involved in filopodial extensions in other cell types.

Genetic analysis in *Chlamydomonas* has shown that the 8-kDa subunit of Dynein (DLC1/LC8) is involved in multiple steps of axoneme assembly and flagellar growth. It is required to maintain the retrograde IFT (Pazour *et al*., 1998), and the assembly of Dynein arms and radial spoke structures of the axoneme (Yang *et al*., 2001). Studies in *Aspergillus* have shown that the NUDG/LC8 is required to maintain nuclear migration, cell growth, and distal end localization of Dynein at higher temperature (Beckwith *et al*., 1998; Liu *et al*., 2003), and studies in *Drosophila* suggested that both DLC1 (*ctp*) and $P150^{Dynactin}$ (*Glued*) are involved in maintaining axonal growth in sensory neurons (Phillis *et al*., 1996; Murphey *et al*., 1999). Together, these data suggest that DLC1/LC8 is required for cell growth in a variety of different cell types.

Article published online ahead of print. Mol. Biol. Cell 10.1091/mbc.E03–11–0848. Article and publication date are available at www.molbiolcell.org/cgi/doi/10.1091/mbc.E03–11–0848.

[V] Online version of this article contains supporting material. Online version is available at www.molbiolcell.org.

* Corresponding author. E mail address: krishanu@tifr.res.in.

Abbreviations used: DLC1, dynein light chain 1; EC, elongation cone; LC8, 8-kDa dynein light chain subunit of *Chlamydomonas*.

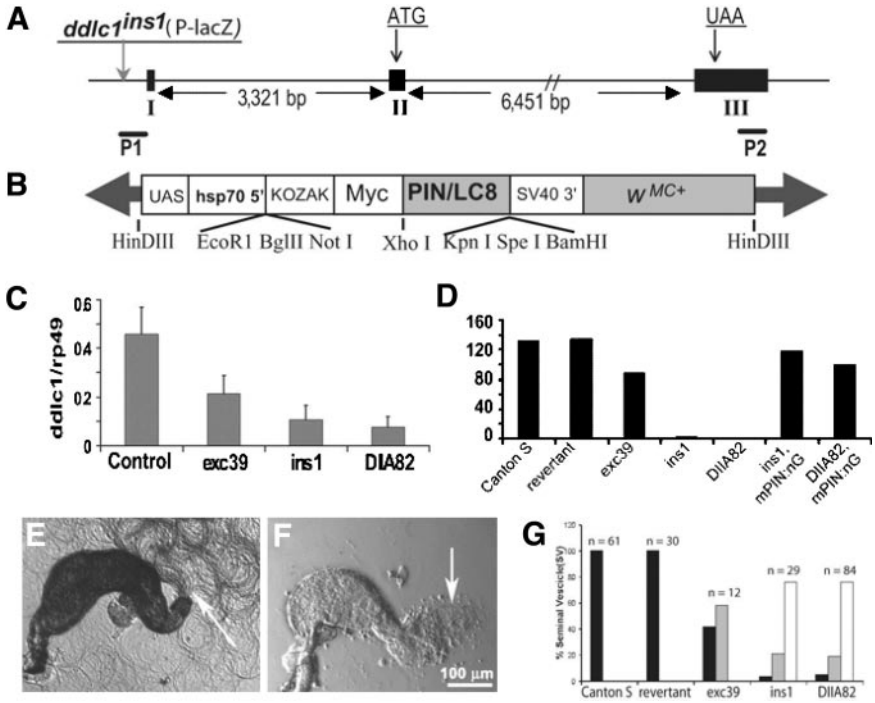

Figure 1. Reduced levels of Ddlc1 cause temperature sensitive recessive lethality and male sterility. (A) Schematic shows the relative positions of exons (I, II, and III), the start (ATG) and stop (UAA) codons in Ddlc1 gene. The positions of the P-lacW insertion in *ddlc1*^{ins1} (vertical gray arrow) and the Ddlc1 specific primers (P1 and P2) are also indicated. (B) Schematic map of the Myc-PIN/LC8 transgene cloned in pPUAST. (C) Histogram represents relative fluorescence intensity of the Ddlc1 amplicons with respect to the rp49. Error bar indicates ± SD, and N ≥4 for all data points. (D) Histograms represent average progenies per wild-type and mutant males, respectively. mPIN:nG represents the presence of UAS-MycPIN/LC8 and nos-Gal4-VP16, and N = 20 or more single male crosses for each bar. (E and F) Seminal vesicles isolated from wild-type control (E) and *ddlc1*^{DIIA82} hemizygous (F) males. Arrow indicates bundles of active sperms in E and a few motile sperms in F. (G) Histograms indicate percentage of distribution of seminal vesicles (SV) in wild-type controls and in different *ddlc1* alleles with a large number of motile sperm (black filled bars), relatively fewer (gray filled bars), and no (white filled bars) motile sperm. All the seminal vesicles from Canton S and *ddlc1*^{rev} adults were filled with vigorously motile sperm (see Supplemental Movie 1), whereas the ones from ddlc1 hemizygous adults were partly filled with relatively sluggish sperm (see Supplemental Movie 2).

DLC1/LC8 represents a conserved family of small (89-aa) polypeptides, which was purified with axonemal and cytoplasmic Dynein complex from the *Chlamydomonas* flagella and mammalian brain, respectively (King and Patel-King, 1995; King *et al*., 1996). Later, homologous proteins were independently identified in *Drosophila* (called DDLC1) and from human cDNA libraries (Dick *et al*., 1996). The human homologue (also known as PIN) was shown to inhibit the neuronal nitric-oxide synthase activity in vitro (Jaffrey and Snyder, 1996). Crystal and the solution structures of this protein (Tochio *et al*., 1998; Liang *et al*., 1999) revealed that it forms a dimer and associates with a consensus five- to six- amino acid-long target peptide (Lo *et al*., 2001). Such peptide sequences are present in different proteins (Rodriguez-Crespo *et al*., 2001), including the 74-kDa intermediate chain (IC74) subunit of Dynein motor complex (Lo *et al*., 2001; Makokha *et al*., 2002). Because DLC1/LC8 also interacts with several proteins outside the Dynein–Dynactin complex (Epstein *et al*., 2000; Herzig *et al*., 2000; Naisbitt *et al*., 2000; Raux *et al*., 2000; Shcnorrer *et al*., 2000), it is likely to act as generic cargo adapter for Dynein.

In this article, we present the results of a cellular and genetic analysis of *ddlc1* function in spermatogenesis to indicate that DDLC1 is required at the growing ends of spermatids to maintain their growth in a Dynein-Dynactin–dependent manner, but surprisingly it seems to have no role in the axoneme assembly. This established that the growth of spermatid tail and that of the axoneme inside involve two independent mechanisms, and Dynein-Dynactin–mediated transport is likely to play a novel role in membrane deposition process during spermatogenesis in *Drosophila*.

MATERIALS AND METHODS

Isolation of New ddlc1 Alleles, Mapping, and Complementation Analysis

All fly stocks were maintained on standard *Drosophila* cornmeal agar, and sucrose medium at 25°C. Description of all the stocks, unless otherwise mentioned, is available in Flybase (www.flybase.org). New *ddlc1* alleles were generated by remobilization of the P-lacW element inserted at the 5′ end of *ddlc1* (Figure 1A) in the *w ddlc1*^{ins1}*/Y; Sb* Δ2–3ry^{+} "jumpstarter" males, which were crossed to C(1)RM y *w f* females, and subsequently the F1 males were screened for thin bristle (tb) and erect wing (ew) traits. A screen of 750 F1 males yielded nine complete revertants (white eyes) with wild-type characteristics, nine P-lacW reinsertion lines (orange eyes) with relatively stronger phenotypes, and three imprecise excision (white eyes) lines with milder phenotypes. They were mapped by meiotic recombination by using the *y w cv v f* chromosome and by noncomplementation tests using the existing *ddlc1* mutant stocks and various other deletion stocks known to uncover the 4C-E region of the salivary gland polytene chromosome (Table 1).

Semiquantitative Reverse Transcription-Polymerase Chain Reaction

Total RNA was isolated from the abdomen of 2-d-old adult males by using a QIAGEN kit (QIAGEN, Valencia, CA). About 50 dissected abdomens were used for each preparation. cDNA was prepared from the isolated total RNA by using avian myeloblastosis virus reverse transcriptase (Roche Diagnostics, Indianapolis, IN) and the 600-base pair Ddlc1-specific fragment was amplified from the cDNA pool by using 5′-GGGGTACCGCAAAACGTTCAGTT-GTG-3′ (P1) and 5′-GCTCTAGACTCTAGATCCTCATCCTC-3′ (P2) (Figure 1A). An additional set of primers was used to amplify the 230-base pair rp49-specific fragment from the same pool. The amplicons were separated in 1.2% agarose gel after 18, 20, 22, 24, 26, and 28 cycles and observed by ethidium bromide staining. Images were captured by a UVP Gel-Doc system (UVP, Inc., Upland CA), and relative intensities of the DNA bands were measured by using LabWorks software (UVP, Inc.). The Ddlc1-specific band became visible at 22 cycles in wild-type control, and the amplification followed the expected binomial increments until 26 cycles.

Transgenic Constructs and Transformation of Fly Stocks

Two different transgenic constructs were made in P-transposon vectors. The MycPIN transgene was made by amplifying the 270-base pair PIN/LC8 open reading frame (ORF) from the cDNA clone (Liang *et al*., 1999) by using specific

Table 1. Description of *D. melanogaster* stocks used in this study

Stocks	Description	Source
ddlc1^{exc6}	Amorphic recessive lethal allele of Ddlc1	Dick *et al*, 1996
ddlc1^{exc39}	Hypomorphic excision allele of Ddlc1	This Study
ddlc1^{ins1}	Hypomorphic insertion allele of Ddlc1	Dick *et al*, 1996
ddlc1^{DIIA82}	Hypomorphic insertion allele of Ddlc1	This Study
Df(1)bi-DL1	Deletion (4A3-5; 4C5-D1), failed to complement *ddlc1*	Bloomington Stock Center
Df(1)bi-D2	Deletion (4B6-C1; 4D7-E1), failed to complement *ddlc1*	Bloomington Stock Center
Df(1)Jc70	Deletion (4C11-12; 5A3-4), complemented the "ew" trait of *ddlc1* alleles	Bloomington Stock Center
W^{1118}; P(MycPIN/LC8)	UAST-MycPIN/LC8 transgene in Chromosome 2	This Study
W^{1118}; P(DDLC1)	UASP-Ddlc1 transgene in Chromosome 2	This Study
Gl^{1}	Antimorphic allele of P150-Dynactin	Bloomington Stock Center
Df(3L)fz-GF3b	Deletion (70B; 70C6) uncovers *Glued*	Bloomington Stock Center
Dhc64C$^{4-19}$	Amorphic allele, Cytoplasmic DHC	Bloomington Stock Center
Df(3L)GN24	Deletion (63F04-07; 64C13–15) uncovers *Dhc64C*	Bloomington Stock Center

primers and cloned into the *Xho*I and *Kpn*I sites of a pPUAST-EP vector (Figure 1B), which is a modified pPUAST with a 17-aa N-terminal Myc epitope coding cassette cloned into the multiple cloning site between the *Not*I and *Xho*I sites. This created a new ORF coding for a Myc-PIN/LC8 fusion protein under the Gal4 inducible (UAS) promoter (Figure 1B). The PUASp-Ddlc1 transgene was made by cloning a 600-base pair Ddlc1 cDNA fragment containing a part of the 5′-untranslated region and ORF into the *Kpn*I and *Xba*I sites of a pPUASp vector (Rorth, 1998). The primer set 5′-GCTCGAGAT-GTGCGACCGGAAG-3′ and 5′-GACAAGTTTAGACCAATTCCATGGCC-3′ was used for amplifying the PIN/LC8 cDNA fragment, and 5′-GGGGTAC-CGCAAAACGTTCAGTTGTG-3′ and 5′-GCTCTAGACTCTAGATCCT-CATCCTC-3′ for amplifying the ddlc1 cDNA fragment. Both these clones were amplified in bacteria and the purified DNA (~1 μg/μl) was microinjected into *y w*; *Ki* Δ2–3ry^{+} embryos. Several stable transformant lines were obtained, which were then used for the genetic rescue experiments. Two different tissue-specific Gal4-expression stocks, Gal4^{daG32} and nosGal4-VP16 were used to express these transgenes. The Gal4^{daG32} is reported to express in all cells during development (Wodarz *et al*., 1995), whereas the nosGal4-VP16 expresses only in the germline cells (Van Doren *et al*., 1998).

Male Sterility and Sperm Motility Assay

Virgin males were stored for 2 d and then each one was mated with five wild-type virgins in separate vials. The total progeny from 10 such crosses were scored after 10–12 d, and average progeny per male was calculated. To further assay the sperm motility, testes and seminal vesicles are dissected from the control, and mutant males in Robb's minimal saline, gently squashed under a coverslip, and observed immediately in a phase contrast microscope.

Immunostaining Techniques

Testes were prepared for immunofluorescence staining by a method described previously (Hime *et al*., 1996). In brief, samples were dissected in 50 mM phosphate buffer (pH 6.7) containing 80 mM KCl, 16 mM NaCl, and 5 mM $MgCl_2$ and fixed at [minus[20°C in 95% ethanol for 5 min and then in 4% paraformaldehyde (Sigma-Aldrich, St. Louis, MO) in phosphate-buffered saline (PBS) for 20 min at room temperature. For isolating cysts, the dissected testes were placed on a plus-charged slide, the apical tip was pierced using a fine needle to release the elongating stage cysts, and then a coverslip was placed on top. After this, the whole assembly was immediately frozen in liquid nitrogen. The coverslip was removed using a razor blade under the frozen condition, and the tissue was fixed as described above. Fixed testes/cysts were washed twice for 15 min each in PBS + 0.3% Triton X-100 (PBT) before the incubation in primary antibody solutions (1 h at room temperature), and then rinsed four times with PBT, and once again incubated for 1 h in secondary antibody solutions. After several further washes in PBT, they were incubated with 1 μg/ml 4,6-diamidino-2-phenylindole or Sytox Green (Molecular Probes, Eugene, OR), rinsed in PBT, and then mounted under a coverslip by using antifade mounting media (Slow fade; Molecular Probes). For DiOC6 (3,3-dihexyloxacarbocyanine iodide) staining, the adult testes were dissected in PBS containing 0.5 μm DiOC6, incubated for 5–15 min, washed in PBS, and then mounted with a drop of PBS. They were observed live. The fluorescent and differential interference contrast images were collected using a Radiance 2100 laser scanning confocal microscope (Bio-Rad, Hercules, CA) and digitally processed using ImageJ and Adobe Photoshop.

Elongation Cone (EC) Distribution Assay

ECs were observed by imaging intact fixed testis stained with α-spectrin antisera. Serial optical sections of the whole testis were collected using a 40× 1.2 numerical aperture objective and Radiance 2100 laser scanning confocal microscope. Stored images were further analyzed using ImageJ. The apical one-half of each testis was divided in four ~0.3-mm sectors along its length, and total number of ECs was counted in each sector. Simultaneously, it was verified whether those ECs were intact or deformed. Mann-Whitney *U* test was performed to get the statistical significance of the change in EC deformity values among different genotypes. Similarly, the %EC distribution was calculated by averaging the ratios between the total number of ECs within a zone and total ECs in the testis, and a parametric test (analysis of variance) was applied to measure statistical significance of the difference between two comparable data sets. All the statistical analyses were performed using GraphPad Insat.

Antibodies

A mouse polyclonal was raised against a DDLC1-specific peptide (12-aa in length) as described previously (Dick *et al*., 1996), and we have raised a rat polyclonal antiserum against the bacterially expressed DDLC1 protein by using standard protocols (Harlow and Lane, 1984). Both antisera were used at 1:200 dilution for immunostaining the tissues and at 1:1000 for Western blots. It recognized a ~10-kDa band in the total protein extracts from wild-type adult testis, which were absent in *ddlc1^{ins1}* hemizygous testis. The rabbit anti-β-spectrin (Dubreuli *et al*., 1997) and anti-α-tubulin (Sigma-Aldrich) were used at 1:100, and a monoclonal for the α-spectrin (mAb3A9; Dubreuil *et al*., 1987) and the β-tubulin (mAbE7; Chu and Klymkowsky, 1989), both obtained from the Developmental Studies Hybridoma Bank (University of Iowa, Iowa City, IA) and used at 1:50 dilutions. The mouse monoclonal anti-DHC (Sharp *et al*., 2000) was used at 1:10 and the rabbit anti-Glued (Fan and Ready, 1997)

Table 2. Genetic noncomplementation test amongst the remobilized *ddlc1^{ins1}* stocks identified different categories of hypomorphic alleles

ddlc1 alleles	exc39	exc123	DIIB14	exc41	DIA5	ins1	DIIA82	exc6	Df(1)bi-Dl1	FM7
exc39	+	+	+	+	+	+	+	ew, tb	ew, tb	+
exc123		+	+	+	+	+	+	ew, tb	ew, tb	+
DIIB14			ew,tb	ew,tb	ew,tb	ew,tb	ew,tb	ew, tb	ew, tb	+
exc41				ew,tb	ew,tb	ew,tb	ew,tb	ew, tb	ew, tb	+
DIA5					ew,tb	ew,tb	ew,tb	ew, tb	ew, tb	+
ins1						ew,tb	ew,tb	ew, tb	ew, tb	+
DIIA82							ew,tb	ew, tb	ew, tb	+
exc6								lethal	lethal	+
Df(1)bi-DL1									lethal	+
FM7	Weak			Moderate			Strong			+

at 1:200, respectively. All the fluorescent conjugated secondary antisera were obtained from Jackson ImmunoResearch Laboratories (West Grove, PA) and used at 1:500 dilutions.

Electron Microscopy

Testes were dissected from 2-d-old adults and fixed by immersion overnight at 4°C in a fixative containing 2.5% glutaraldehyde and 2.0% paraformaldehyde and 0.04% $CaCl_2$ in 0.1 M phosphate buffer at pH 7.4. The $CaCl_2$ provides increased membrane stabilization. Testes were washed in phosphate buffer, postfixed with OsO_4, dehydrated in an ethanol series, and embedded in Araldite. Ultrathin sections (100 nm) were stained with aqueous uranyl acetate and lead citrate and examined with a JEOL electron microscope.

RESULTS

Partial deletions of ddlc1 gene led to early embryonic lethality and the homozygous mutant clones were cell lethal (Dick *et al*., 1996). A P-transposon inserted 40 base pairs upstream to the ddlc1 transcript (*ddlc1^{ins1}*; Figure 1A) was partly viable but caused visible recessive phenotypes such as thin bristles (tb), abnormal wing-veins, and female sterility, and we found that the mutant flies have erect wings (ew) as well. We also noticed that *ddlc1^{ins1}* hemizygous males are sterile, and simple microscopic analysis of their testes showed that the spermatids were abnormally coiled in the cysts. Because DDLC1 is likely to act in a multisubunit complex, the stoichiometry of this protein could determine its functions in the cell. Therefore, we decided to estimate its role in different cellular processes by using a graded series of hypomorphic alleles.

Genetic Characterization of ddlc1 alleles

To generate alleles of different genetic strengths, we remobilized the P-lacW insertion in *ddlc1^{ins1}* (Figure 1A) and isolated several insertion and excision alleles. Meiotic recombination mapping placed the mutations in the reinsertion and excision stocks causing the "ew" and "tb" traits between *w* and *cv* loci, and noncomplementation tests with various deletions (Table 1) mapped them between the salivary chromosome bands 4B6 and 4C11-12 of the X-chromosome. The genetic noncomplementation tests among these alleles further suggested that they belong to a single group along with the known *ddlc1* alleles. However, the newly generated *ddlc1* alleles were found to have different intensities of "ew" and "tb" traits, and thus they were grouped into three hypomorphic classes with ascending grades of severity (Table 2). We selected *ddlc1^{exc39}* from the weak, *ddlc1^{ins1}* from the intermediate, and *ddlc1^{DIIA82}* from strong hypomorphic class, respectively, for further quantification of their phenotypes. The measurement of relative viability of hemizygous mutant males and homozygous females (Table 3) further confirmed that these are hypomorphic alleles of varying strengths. Interestingly, we also noted that the extent of viability in different *ddlc1* alleles was further reduced when the stocks were grown at an elevated temperature (Table 3).

The *ddlc1* alleles described above were generated by remobilization of a single P-lacW insertion at the 5′ end of ddlc1 coding sequence. P-transposon insertions at the 5′ ends of genetic elements were known to inactivate gene expression downstream (Spradling *et al*., 1995, 1999). Often remobilization of P-transposons either leaves a fragment of the element in its primary insertion site, or causes extensive reorganization and sometimes deletion of the flanking genomic sequences, leading to a partial/complete inactivation of the downstream/flanking genes (Voelker *et al*., 1984; Daniels *et al*., 1985, Zhang and Spradling, 1993; Delattre *et al*., 1995; Timakov *et al*., 2002). Therefore, the hypomorphic defects observed in *ddlc1* alleles are likely to be caused by reduced ddlc1 gene expression. To confirm that, we estimated relative levels of the Ddlc1 mRNA in the mutant tissue with respect to that of the rRNA rp49 by semiquantitative reverse transcription-polymerase chain reaction analysis. This revealed that levels of Ddlc1 transcripts were reduced in *ddlc1^{exc39}*, *ddlc1^{ins1}* and *ddlc1^{DIIA82}* (Figure 1C), and the order of reductions correlated well with that of the viability indices. Together, these suggested that the recessive phenotypes of the *ddlc1* alleles are caused by partial reduction in the gene expression and the phenotypic severity is proportional to the level of reduction.

Table 3. Relative viability indices of ddlc1 alleles

	Allele					
Temp.	*ddlc1^{exc39}*/ *ddlc1^{exc39}*	*ddlc1^{ins1}*/ *ddlc1^{ins1}*	*ddlc1^{DIIA82}*/ *ddlc1^{DIIA82}*	*ddlc1^{exc39}*/ Df(1)biDL1	*ddlc1^{ins1}*/ Df(1)biDL1	*ddlc1^{DIIA82}*/ Df(1)biDL1
25°C	*100*	*93*	*51.73*	*89.7*	*63.7*	*38*
29°C	*100*	*20*	*0.0*	*87.2*	*0.0*	*0.0*

Table 4. Ectopic expression of the myc-PIN/LC8 as well as DDLC1 rescues the recessive lethality of *ddlc1*^{exc6}

	ddlc1^{exc6}/Y	**ddlc1^{exc6}/Y, daG32/+**	*FM7c y w B/Y*	*FM7c y w B/Y,* daG32/+
MycPIN	*0*	**80**	*47*	*61*
DDLC1	*0*	**42**	*12*	*29*

Finally, to confirm that these phenotypes are indeed caused by the loss of DDLC1, we used two different transgenic fly stocks carrying PUASp-Ddlc1 and PUAST-Myc-PIN, respectively. PIN/LC8 is 95.5% identical to the predicted DDLC1 protein, and ectopic expression of both Ddlc1 and Myc-PIN by Gal4^{daG32} in *ddlc1*^{exc6} hemizygous background completely rescued the lethality (Table 4) as well as the thin bristle and the erect wing phenotypes. *ddlc1*^{exc6} is a recessive lethal allele (Dick *et al*., 1996), which failed to complement all the newly generated alleles described above. Therefore, the rescue of *ddlc1*^{exc6} lethality by targeted expression of Ddlc1 and Myc-PIN mapped the cause of lethality to the Ddlc1 locus.

DDLC1 is expected to interact with the Dynein and several other protein complexes. To identify its cellular functions in such different contexts by using genetics, we needed some easily quantifiable traits other than lethality. We found that *ddlc1* hemizygous males were poorly fertile (Figure 1D) and the seminal vesicles of *ddlc1*^{ins1} and *ddlc1*^{DIIA82} hemizygous males (Figure 1F) were mostly empty or sometimes contained relatively lesser numbers of motile sperm (Figure 1G). The mutant sperms also seemed to be less active (see supplemental movies). These defects were rescued by a germline-specific expression of the Myc-PIN fusion protein by the nosGal4-VP16 driver, suggesting that Ddlc1 is required in gonial cells to maintain spermatid development.

Spermatids Are Abnormally Coiled at the Growing Ends in ddlc1 Hemizygous Testis

Spermatogenesis is well recognized as an excellent system to study mechanisms of cell growth and differentiation. It starts with the formation of a gonial cell at the apex of the testis, which undergoes four mitoses and one meiotic division to form 64 spermatids, which remain encapsulated by two somatic cyst cells (Fuller 1993). The spermatids then mature and form distinctly identifiable onion stage structures (Figure 2A) where each spermatid nucleus (Figure 2A, arrow) is associated with a large spherical mitochondrion (Figure 2A, arrowheads) known as Nebenkern. Then, they grow into cylindrical spermatids, which seem uniformly bundled (Figure 2C, arrowheads) inside the cyst envelope with a membranous bulge at their distal ends (Figure 2C, arrow). In 2-d-old *ddlc1*^{exc39} hemizygous testes, the onion stage cysts had normal Nebenkern and nuclear pairing (Figure 2B), but the distal ends of spermatids were abnormally coiled inside the cysts (Figure 2D, arrow). This defect was more severe in the other alleles, the cysts seemed shorter, and there were fewer such cysts in each testis. Serial sectioning further confirmed this defect in intact testis. The control cysts contained 63.8 ± 1.0 (N = 9) evenly packed spermatids (Figure 2E, arrowheads), whereas they were irregularly bundled in *ddlc1* testes, and it was difficult to count their number. Often we noticed multiple spermatid bundles (Figure 2F, arrowheads) within a single cyst envelope. This could arise due to abnormal twisting of the spermatid bundle within the cyst.

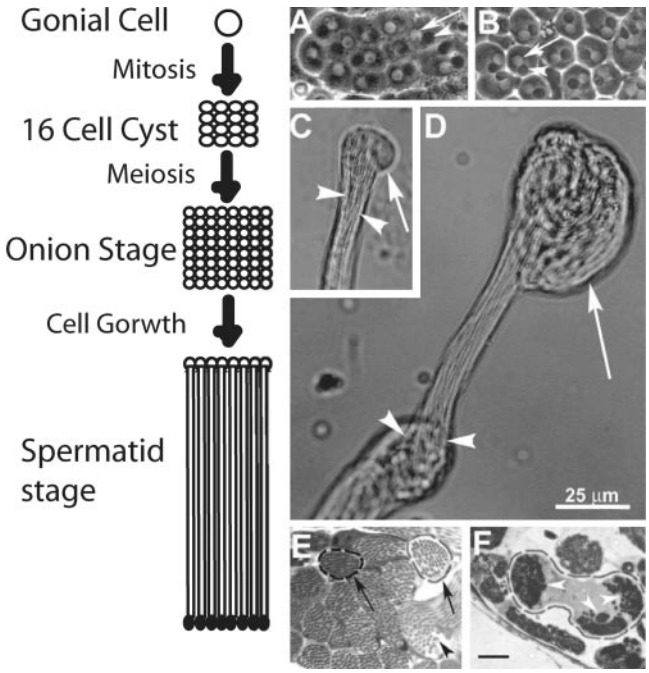

Figure 2. Ddlc1 is essential for proper growth of sperm tails in developing cysts. (A–D) Phase contrast images of isolated cysts from wild-type control (A and C) and *ddlc1*^{exc39} hemizygous (B and D) testes. (A and B) Onion stage spermatocytes isolated from the wild-type control (A) and mutant testes (B), respectively. The arrows and arrowheads indicate nuclei and onion stage mitochondria, respectively. (C) Distal end of an elongating cyst from wild-type control testis. The spermatid tails (arrowheads) are tightly bundled and have a membranous bulge (arrow) at their distal ends. (D) Spermatids are abnormally knotted (arrowheads) in the middle and coiled (arrow) at their distal ends inside the cysts in *ddlc1* testis. Scale is equal for all figures and as indicated in D. (E and F) Thin sections (1 μm) of testis from the wild-type control (E) and *ddlc1*^{DIIA82} (F) adults stained with methylene blue. (E) Two typical cyst boundaries (arrows) are marked, and the arrowhead indicates a single spermatid. (F) Spermatids are abnormally bundled (arrowheads) in multiple fascicles even within a single cyst. Bar, 10 μm for E and F.

Such disorganization was also observed in rnRacGAP mutants of *Drosophila* (Bergeret *et al*., 2001), which caused severe coiling of axonemes at the distal ends due to reduced spermatid growth. Therefore, our results indicate that Ddlc1 is required for uniform growth of spermatids inside a cyst, which is further resolved by a quantitative assay of spermatid growth in the mutant testis as described below.

Growing Ends of Spermatids Are Encapsulated by a Spectrin-rich Scaffold Derived from Postmeiotic Fusome

Spermatids remain linked with each other through ring canals while growing, and the spectrin scaffold of fusomes convert into a honeycomb-like structure at the growing end of the cyst (Hime *et al*., 1996). The elongation phase lasts for several hours, and at any given time at least 25 cysts of different lengths were found in a wild-type testis (Lindsley and Tokuyasu, 1980). Immunostaining of isolated wild-type cysts by using α- and β-spectrin as well as α- and β-tubulin antisera confirmed that the spectrin cytoskeleton of the fusome (Figure 3A, arrows) reorganizes into cylindrical scaffolds (Figure 3C, arrows) at the growing ends of individual axonemes (Figure 3D, 1–4), and together they form a hon-

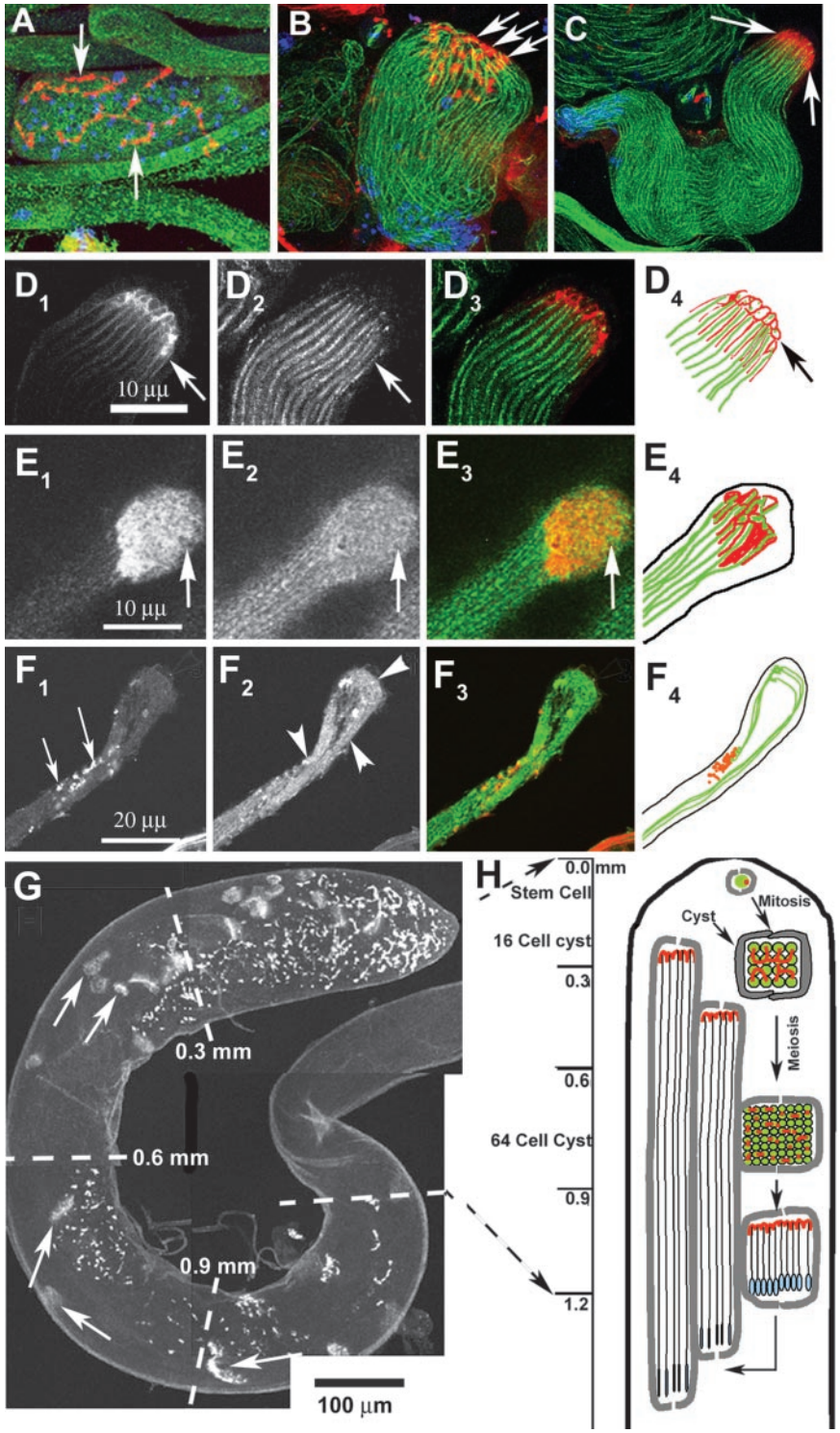

Figure 3. Spectrin scaffold of fusomes is reorganized to form the cylindrical spectrin caps at the growing ends of axoneme. A–D show anti-β-spectrin (colored red) and anti-β-tubulin (colored green) staining in developing spermatids of wild-type testis. The nuclear DNA (colored blue) is stained using Sytox Green. (A) Postmeiotic stage cyst with regular organization of fusomes (arrow) and 64 nuclei inside. (B) Elongating stage cyst with the spermatid heads (blue) bundled together at one end and condensed spectrin staining (arrows) at the other end. The axonemal microtubules (green) are marked by anti-β-tubulin. (C) The β-spectrin staining (arrows) at the growing ends of axoneme seems compact at a later stage, and the spermatids also seemed uniformly bundled. (D1–4) Bundle of cortical spectrin-rich structures (arrows in D1) is visible at the distal end when the cyst is between 1.5 and 2 mm in length, and each one seems to cap individual axoneme (arrows in D2). A red green merge of D1 and D2 is presented in D3, and D4 shows a tracing of individual axoneme (green) and the spectrin caps at this stage. (E1–4) Distal end of a wild-type cyst stained with α-spectrin (E1) and α-tubulin (E2), respectively. Arrows indicate the distal end in E1–3 and E3 shows a red green merge of E1 and E2. A tracing of α-spectrin and α-tubulin staining is shown in E4. (F1–4) Similar staining in *ddlc1*^{ins1} cyst shows that the spectrin-rich honeycomb structure is deformed into punctate spots (F1, arrows) and abnormally twisted axonemes (F2, arrowheads). (G) Anti-α-spectrin staining of intact testis depicts a regular distribution of the spectrin scaffolds (arrows) along its length. These are called elongation cone (EC) in this study. (H) Illustration indicates the orientation and position of the spermatid heads (blue) and the spectrin scaffolds (red) within a cyst at different stages of spermatogenesis inside the testis.

eycomb-like structure (Figure 3, D1 and E1, arrow), which marks the growing ends of all the elongating spermatids in a cyst. We will now refer to this as the EC for the convenience of further description. We found that the spectrin cytoskeleton of the ECs was deformed and often missing in *ddlc1* cysts (Figure 3F1, arrow), and the tubulin cytoskeleton of the spermatids, consisting of mainly the axoneme and some cellular microtubule filaments at the distal ends, was abnormally coiled (Figure 3F2). This suggested that Ddlc1 is required to maintain the spectrin cytoskeleton of the ECs, which is likely to play an important role in regulating the spermatid growth at the distal end.

Analysis of the EC distribution profile along the length of the testis (Figure 3G, arrows) further established that they form ~1.2 mm from the apex, and then they grow back toward the apex (Figure 3H). A wild-type testis from a 2-d-old adult male contained 29.7 ± 1 (N = 7) ECs (Figure 4A), and they were distributed in a typical manner along the

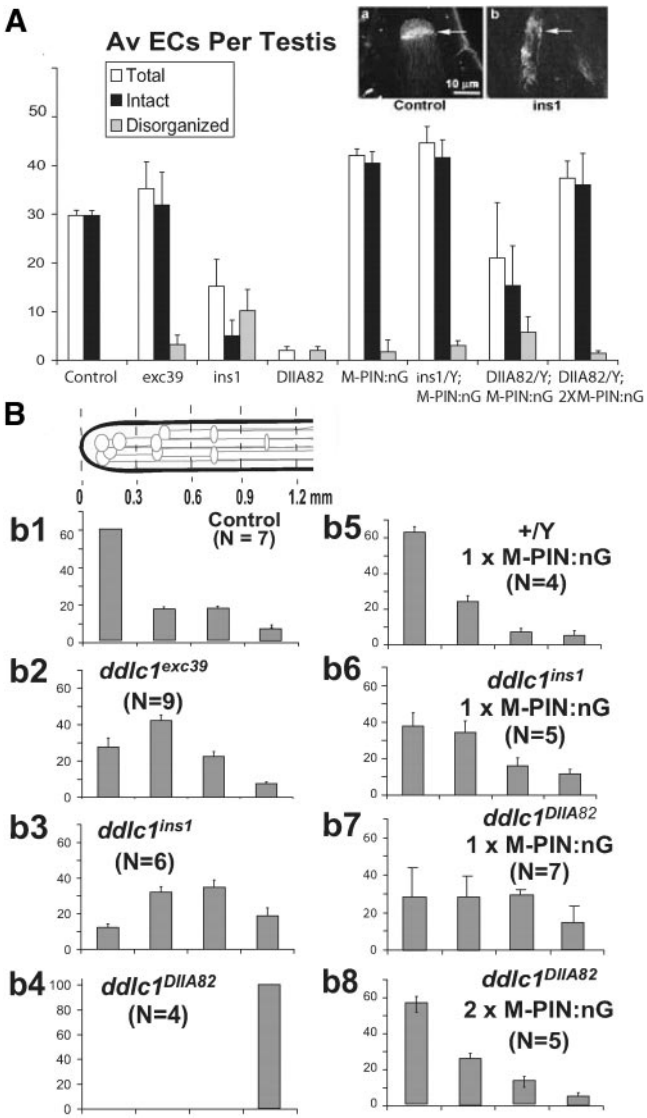

Figure 4. Mutations in the ddlc1 locus disrupt elongation cone formation and reduce spermatid growth. (A) Histogram depicts average number of recognizable intact and disrupted EC in wild-type control and mutant testes. Error bars indicates ± SD, and N = 4 or more for each data set. The insets show typical examples of an intact (arrow in a) and a disorganized (arrow in b) elongation cones revealed by anti-α-spectrin staining. (B) Schematic at the top left corner indicates the apical one-half of a testis, and gray lines with elliptical heads indicate ECs of individual cysts. The set of histograms (b1–b8) represent percentage of EC distributions ± SD in different length segments of the testis as indicated in the schematic. The scale is set from the apical tip of the testis, and the length segments are indicated in millimeters. MPIN:nG indicates the presence of UAS-Myc-PIN/+; nosGal4-VP16/+ in the background.

apical one-half of a testis. Because ECs are present at the growing ends of cysts, their positions along the testis should reflect the relative distribution of cyst lengths in the testis. To estimate that, we divided the apical one-half of the testis into four equal segments and counted the distribution of ECs in each of them, and the profile is presented in a normalized scale as percentage of total ECs in the testis (Figure 4Bb1). A majority of the ECs were found at the apical segment, whereas the rest were distributed in a decreasing order in successive segments below that. These data indicate that cysts initially grow at a faster rate, which slows down as they approach the final length. Therefore, we used this assay further to estimate relative cyst lengths in *ddlc1* testes.

Loss of ddlc1 Disrupted the ECs and Reduced Spermatid Growth in the Testis

Both $ddlc1^{ins1}$ and $ddlc1^{DIIA82}$ hemizygous testes had significantly reduced numbers of ECs, and many of them were deformed (Figure 4A). The reduction in average EC numbers and the extent of their deformity was directly proportional to the reduction in the level of Ddlc1 mRNA in these mutants. This established that the stoichiometry of DDLC1 protein is important for the formation and maintenance of spectrin cytoskeleton in the ECs. We also noticed that the peak of the EC distribution profile was shifted to the next segment (0.3–0.6 mm) in $ddlc1^{exc39}$ (Figure 4Bb2) and even further down in $ddlc1^{ins1}$ (Figure 4Bb3) and $ddlc1^{DIIA82}$ (Figure 4Bb4) hemizygous testes. This indicated that average cyst lengths are shortened in *ddlc1* testes, which could happen due to a retarded or abnormal spermatid growth. This was particularly clear in $ddlc1^{exc39}$ testes, which contained nearly wild-type levels of intact ECs, but their distribution was shifted to the basal side. It also pointed to the fact that Ddlc1 activity is required to maintain spermatid growth even after the ECs are formed.

We further established that by measuring the rescue of these two phenotypes with different doses of Myc-PIN expression in gonial cells. It showed that a single copy of UAS-Myc-PIN along with the nosGal4-VP16 could rescue the average number of ECs to the wild-type level in $ddlc1^{ins1}$ backgrounds (Figure 4A). However, it was not enough to restore their distribution profiles (Figure 4Bb6). The level of Ddlc1 transcript is further reduced in $ddlc1^{DIIA82}$, and in this background a single copy of UAS-Myc-PIN:nosGal4-VP16 (MPIN:nG) only partially rescued the EC deformity defects (Figure 4A) as well as their distribution profile (Figure 4Bb7). A complete rescue of both the defects was achieved by using two copies of the transgene along with the driver (2 × MPIN:nG) in $ddlc1^{DIIA82}$ background (Figure 4Bb8). The presence of either UAS-Myc-PIN or nosGal4-VP16 alone didn't rescue the defects in *ddlc1* background.

Partial Loss of Dhc64C and Glued in ddlc1 Backgrounds Enhanced the EC Formation and the Spermatid Growth Defects

DDLC1 homologues are known to associate with Dynein complex in different organisms. Therefore, to understand the role of the Dynein–Dynactin complex in DDLC1 functions during spermatogenesis, we measured the effect of partial reduction of Dhc64C and Glued in *ddlc1* backgrounds. The *Df(3l)GN24* and *Df(3L)fzGF3b* were used to measure the effect of reduced dose of Dhc64C and Glued, respectively, on ddlc1 functions, and $Dhc64C^{4-19}$ and $Glued^{1}$ were used to measure specific interactions. We found that the presence of one copy of *Df(3l)GN24*, $Glued^{1}$, or, *Df(3L)fzGF3b* in the background enhanced the male sterility defects of *ddlc1* alleles (Table 5), indicating that Ddlc1 interacts with the Dynein–Dynactin complex. However, the presence of one copy of $Dhc64C^{4-19}$ in the background suppressed this defect (Table 5). This was intriguing because *Df(3l)GN24* had exactly the opposite effect. Nevertheless, these data suggested that DDLC1 interacts with the DHC64C and GLUED. To further understand the role of such interactions during spermatogenesis, we studied the EC formation and cyst length distribution profiles in these mutant combinations. This showed that the presence of a

Table 5. Partial reduction of DHC and Glued enhance the male sterility defects of *ddlc1* alleles

	ddlc1 Alleles							
	+		exc39		ins1		DIIA82	
Other Mutants	% sterile	Average Progeny	% sterile	Average Progeny	% sterile	Average Progeny	% sterile	Average Progeny
+/+	0.0 (n = 50)	132	13.3 (n = 30)	88	50.8 (n = 63)	3	92.0 (n = 60)	<1
Dhc64C$^{4-19}$/+	5.0 (n = 21)	113	11.7 (n = 34)	135	26.5 (n = 49)	54	81.8 (n = 11)	<1
Df(3L)GN24/+ (Dhc64C$^-$)	0.0 (n = 11)	120	11.7 (n = 17)	41	100.0 (n = 6)	0	Poorly viable	
Gl^1/+	7.0 (n = 15)	120	68.8 (n = 45)	8	100.0 (n = 22)	0	Lethal	
Df(3L)fz-GF3b/+ (Gl$^-$)	0.0 (n = 10)	132	80.0 (n = 5)	3	100.0 (n = 5)	0	Poorly viable	

single copy of *Df(3l)GN24*, *Glued^1*, or, *Df(3L)fzGF3b* could significantly enhance the EC deformation defects of various *ddlc1* alleles, and the total ECs per testis were also significantly reduced (Figure 5A). In addition, the average cyst lengths were further reduced as the EC distribution profile was further shifted toward the base of the testis (Figure 5B). The most severe phenotypic enhancements were seen with *Df(3L)fzGF3b*/+ in the background. It almost eliminated detectable ECs in both *ddlc1^{exc39}* and *ddlc1^{ins1}* backgrounds and significantly enhanced the lethality of *ddlc1^{DIIA82}* males. Together, these data suggest that Ddlc1 interacts with the Dynein–Dynactin complex during EC formation and spermatid growth.

Dhc64C$^{4-19}$ is an EMS-induced recessive lethal allele, which failed to complement the null alleles of the Dhc64C locus (Gepner *et al.*, 1996). Interestingly, the allele itself had a mildly dominant effect on the EC stability, as indicated by the large SD of average EC numbers in *Dhc64C$^{4-19}$*/+ testis (Figure 5A), and average cyst lengths were also marginally reduced as the peak of the EC distribution profile was shifted to the basal end (Figure 5Bb7). In *ddlc1* hemizygous backgrounds, it suppressed the EC deformation defects, and the average EC numbers were also increased (Figure 5A). However, it had no detectable effect on the EC distribution profiles of the *ddlc1* alleles (Figure 5Bb8-9). This was very different from the general enhancements seen in other mutant backgrounds. This suggests that *Dhc64C$^{4-19}$* could alter the threshold of Ddlc1 requirement during the EC formation and maintenance process, but not during spermatid growth. Hence, it further indicated that the EC formation and spermatid elongation are two separate cellular functions, although both required the Dynein–Dynactin complex.

DDLC1 Along with the DHC and GLUED Are Enriched at the Distal Ends of the Growing Spermatids

To locate the sites of DDLC1 actions in growing spermatids, we stained isolated cysts with two different antisera raised against DDLC1 in mouse and rat, respectively. The mouse anti-DDLC1 showed relatively higher level of staining at the distal ends of individual spermatids (Figure 6A, arrowheads), which overlapped with the α-tubulin enrichment pattern in this region. Such distal end enrichment was absent in cysts from *ddlc1^{ins1}* testes (Figure 6B), and anti-α-tubulin staining revealed that the axonemes were abnormally coiled inside. An identical staining pattern was observed using the rat-anti-DDLC1 antisera, and higher magnification images of the EC region showed that the DDLC1 is present along the cortical spectrin and F-actin enrichments in this region (Figure 6C, arrows). In addition, we have also seen independent punctate enrichments of DDLC1 in the cytoplasm (Figure 6C, fine arrow). Studies in *nudG* mutants of *Aspergillus* have shown that the protein is enriched at the hyphal tips and it is essential to maintain the

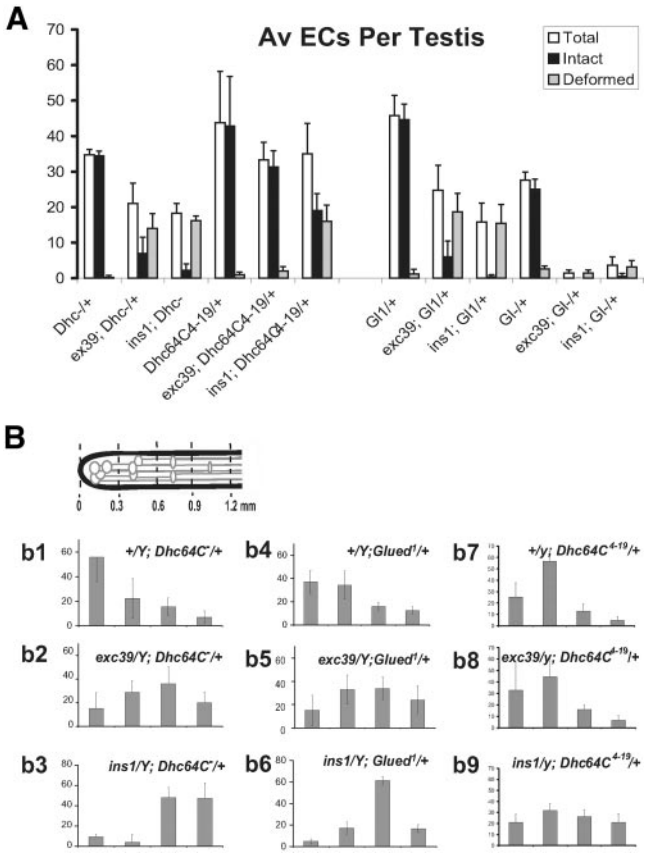

Figure 5. Additional reduction of DHC and Glued enhanced the EC deformation and spermatid growth defects of *ddlc1* alleles. (A) Histogram represents EC morphology parameters counted in different mutant combinations (shown in the x-axis) containing *ddlc1* alleles in the background and as described in the previous figure. The error bars indicates ± SD, and N = 4 or more for each data set. (B) EC distribution profile along the length of the testes for different mutant combinations containing *ddlc1* alleles in the background and as described in the previous figure. The error bars indicate ± SD, and N = 4 or more for each data set. *Df(3L)GN24* is mentioned as DHC$^-$ and *Df(3L)fzGF3b* is mentioned as Gl$^-$ in this figure.

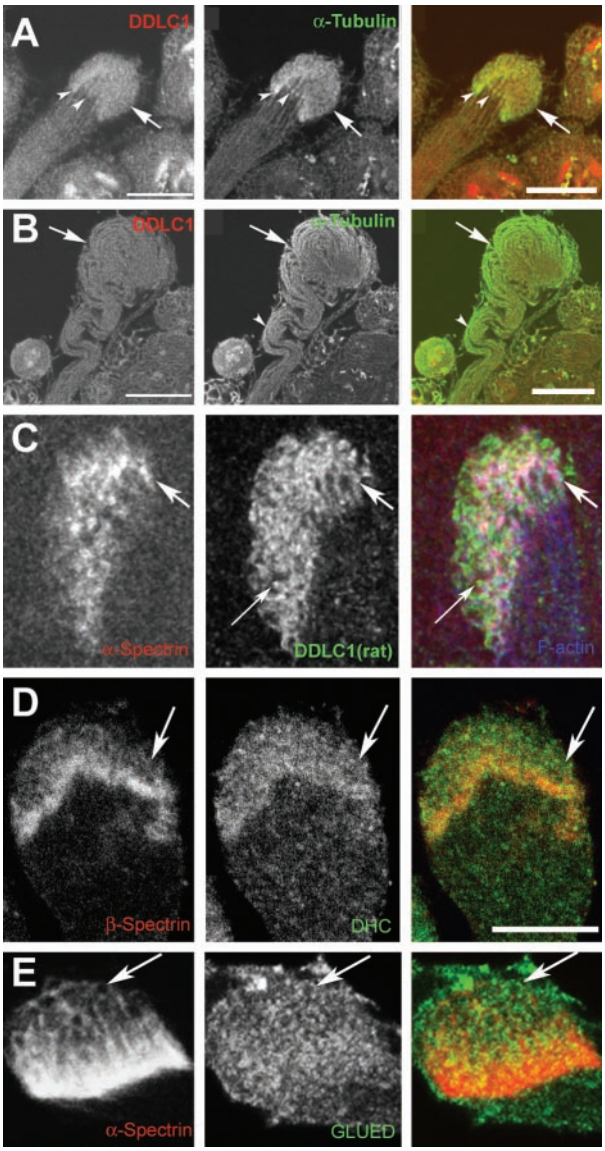

Figure 6. DDLC1 is enriched at the EC region along with DHC and GLUED. Isolated cysts were immunostained with anti-DDLC1 (A–C), anti-DHC (D), and anti-GLUED (E), and the same sample were also stained with anti-α-tubulin (A and B), anti-β-spectrin (D), and anti-α-spectrin (C and E) antisera. (A) In wild-type cyst, the DDLC1 and α-tubulin were enriched at the distal ends of individual spermatids (arrowheads). (B) In *ddlc1*^{ins1} cyst, the DDLC1 enrichment was absent, and the axonemal microtubules seemed abnormally bent in the middle (arrowhead) and coiled at the distal end (arrow). (C) Higher magnification of the EC region stained with anti-α-spectrin (red), rat-anti-DDLC1 (green), and phalloidin (blue) showed enrichment of DDLC1 along the cortical spectrin network of the EC (arrows). In addition, some cytosolic DDLC1-enriched spots were also visible (fine arrow). (D and E) The DHC (D, green) and the GLUED (E, green) antisera also showed punctate staining along the cortical spectrin cytoskeleton in the EC (arrows). Bar, 20 μm in A and B and 10 μm in C–E.

Dynein heavy chain localization in this region as well as the cell growth (Beckwith *et al*., 1998; Liu *et al*., 2003).

Therefore, to determine whether Ddlc1 would have a similar role in *Drosophila*, we stained isolated cysts from wild-type and mutant testes with anti-DHC and anti-Glued antisera, respectively. These stains showed clear enrichment of these two antigens at the distal ends of isolated cysts. The DHC staining seemed to be distributed in the cytoplasm and along the cortical spectrin layer (Figure 6D, arrows), whereas the anti-Glued staining seemed to concentrate in punctate spots along the spectrin cytoskeleton in the EC region (Figure 6E, arrows). Such staining patterns were not visible in *ddlc1*^{ins1} cysts (our unpublished data). Together, all the staining experiments revealed that DDLC1 is also required to maintain DHC and GLUED enrichment at the distal ends of spermatids and identified the site of DDLC1-DHC-Glued action at the distal end of the spermatids.

Mutations in ddlc1 Affect the Cellularization of Individual Spermatids as They Grow, but Their Axoneme Organization Remained Normal

To further understand the cellular mechanism of Ddlc1 action, we studied the ultrastructure of growing spermatids from wild-type control and mutant testes. We always found 64 such axoneme-mitochondria assemblies in every cyst section from the wild-type control testis, and expectedly they were encapsulated in partially formed sheath membrane (Figure 7A, arrowheads) at the caudal end. Higher resolution images of section from the growing tips of spermatids also revealed multiple axoneme-mitochondrial assemblies (Figure 7B, arrow) in syncytium with partly formed multivesiculated axonemal sheath (Figure 7B, arrowheads) in between them. In mature cysts, compacted mitochondrial derivatives and axoneme pairs (Figure 7C, arrow) were invested in separate sheaths. In contrast, the *ddlc1* testis contained some mega cysts with several axoneme-mitochondria pairs within a single membranous envelope (Figure 7D, arrows). But the number of cellular envelopes, including those containing multiple axonemes, was close to 64. Higher magnification images also revealed incompletely formed sheath (Figure 7E, arrowhead) as well as cellular envelopes containing multiple axonemes (Figure 7E, arrows). Furthermore, some apparently matured cysts had incompletely invested spermatids (Figure 7F, arrows) with multiple axoneme-mitochondria pairs inside. Such incompletely formed axonemal sheath suggested abnormal interspermatid membrane deposition process in the mutants. This could block the cell growth and result in the spiraling of axoneme-mitochondrial assembly at the distal ends. Similar phenotypes were observed in rnRacGAP mutants earlier (Bergeret *et al*., 2001). The abnormal investment of the spermatid tails at a later stage further indicates that DDLC1 is also likely to be involved in that process. Similar phenotype was observed in *jar*^{1} (Hicks *et al*., 1999) and *Chc*^{4} (Fabrizio *et al*., 1998) homozygous adults earlier. Alternatively, this could also result because of a faulty membrane deposition process.

Unexpectedly, however, the organization of axonemal microtubule in the mutant spermatids seemed normal. The longitudinal sections showed normal peripheral (Figure 7G, arrowheads) and central (Figure 7G, arrow) axonemal microtubules, which were continuously formed and transverse sections showed the 9 + 2 organization (Figure 7, H and I). The outer (Figure 7H, arrows) and inner (Figure 7H, arrowheads) Dynein arms and the radial spoke structures also seemed normal in these axonemes. In addition, there was no accumulation of electron dense structures around the axoneme as observed in previous studies with *fla14* mutants of *Chlamydomonas* (Pazour *et al*., 1998). We scored for the presence of the 9 + 2 microtubule organization and the radial spoke structures in randomly sampled axonemes from Canton S (278 axonemes), *ddlc1*^{rev} (104 axonemes), *ddlc1*^{ins1} (503 axonemes), and *ddlc1*^{DIIA82} (301 axonemes) testes, and all were normal. These suggested that DDLC1 is unlikely to be

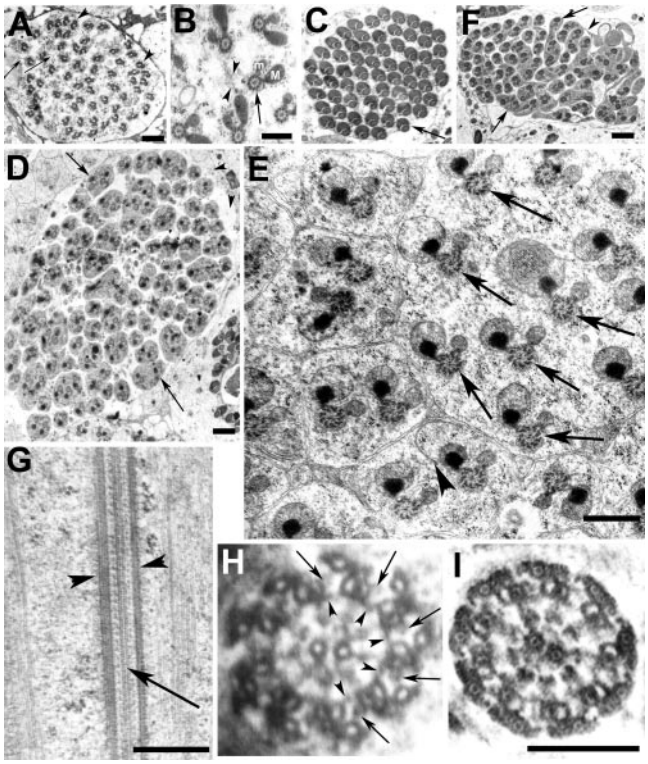

Figure 7. Mutations in ddlc1 affects the cellularization of spermatids. Electron microscopic images of transverse sections of *ddlc1*^{rev} (A–C), and *ddlc1*^{DIIA82} (D–F) testes collected from 2-d-old adults. (A) Section close to the caudal end of a cyst shows 64 axoneme-mitochondria sets mostly wrapped in individual axonemal sheath connected by thin membranous bridges (arrows). But often, more than one axoneme-mitochondria set was found within a single envelope (arrowheads). (B) Axoneme (arrow) and the major (M) and minor (m) mitochondrial derivatives surrounded by cellular microtubules are in syncytium at the caudal most end, and some incompletely formed membrane lamellae with vesicular bodies (arrowheads) attached were seen in this region. (C) Matured cysts showing individually wrapped axoneme-mitochondria pairs (arrow). (D) Mega cyst from *ddlc1*^{DIIA82} testis containing 112 axonemes and with multiple axonemes within a single envelope (arrows). In total, 64 such envelopes were visible in this section. (E) Higher magnification image of a part of a different cyst from the same section shows incompletely formed axonemal sheath (arrowhead) and multiple axoneme-mitochondria sets (arrows) within a single cellular envelope. The morphology of the axoneme-mitochondria complex seemed normal. (F) Section of a seemingly mature cyst from *ddlc1*^{DIIA82} testis showing incompletely individualized spermatids (arrows) with multiple axoneme-mitochondria sets within one envelope and interconnected by thin membranous bridges (arrowhead). (G) Longitudinal section through the axoneme from an immature (preindividualization) spermatid from *ddlc1*^{DIIA82} hemizygous testis revealed normal peripheral (arrowheads) and central (arrow) microtubule assembly. (H) Cross section of an axoneme at the growing end of the spermatid from the same sample revealed 9 + 2 organization of microtubules, the outer (arrows) and inner (arrowheads) Dynein arms, and the radial spoke structures. (I) Section of a relatively matured spermatid (postindividualization) from the mutant testis also showed normal organization. Bar, 1 μm in A, D, and F; 0.5 μm in B, E, and G; and 0.2 μm for H and I as shown in I.

involved in axonemal assembly but required for proper cellularization of individual spermatids, or, alternatively, the amount of the protein present in the hypomorphic alleles used in this study may be sufficient to maintain this process.

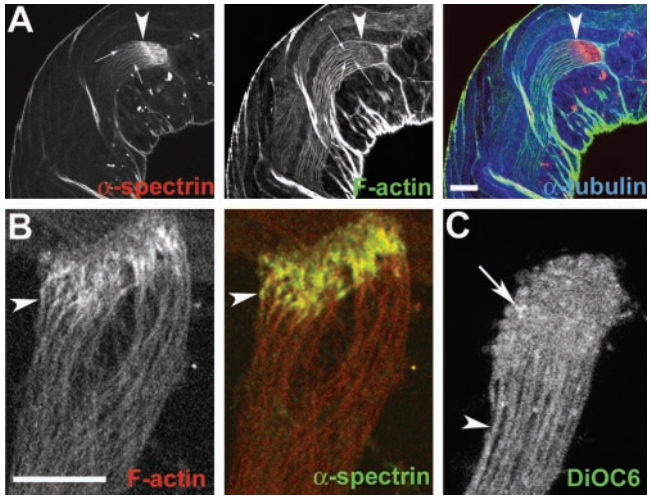

Figure 8. Cortical F-actin assembly is formed around developing spermatids at the EC region. (A) Optical section of an intact adult testis stained with anti-α-spectrin (red), rhodamine isothiocyanate: phalloidin (green), and anti-α-tubulin (blue). Arrowheads indicate the distal end (EC) of a cyst and arrows indicate cortical localization of α-spectrin and F-actin around individual spermatids in the cyst. Note that the cortical F-actin as well as the axonemal α-tubulin staining end at the proximal part of the EC structure. (B) Distal end of an isolated cyst stained with phalloidin (red) and anti-α-spectrin (green). Arrowhead indicates cortical enrichment of F-actin and spectrin at the distal end of a single spermatid. (C) Single optical section of an isolated live cyst stained with DiOC6. Arrowhead indicates a single spermatid cell, and arrow indicates enrichment of staining in individual spermatids at the distal ends.

Axonemal Sheath Forms around Individual Spermatids at the EC Region

The ultrastructure studies of spermatids as presented in this article show that they are already cellularized at the growing ends. However, several previous studies have indicated that the spermatids grow in syncytium and the progression of cystic bulge individualizes them (Fabrizio *et al*., 1996; Rogat and Miller, 2002). Therefore, to confirm that the spermatids are indeed individually wrapped in axonemal sheath as they grow, we immunolabeled intact testes with fluorescently labeled phalloidin, anti-α-spectrin, and α-tubulin antisera. This showed that a cortical F-actin assembly of individual spermatids (Figure 8A, fine arrows; and B, arrowheads) extends right up to the distal end and overlaps with the cortical spectrin enrichments in the EC. A DiOC6 staining of isolated live cysts further showed that the spermatids are completely encapsulated in independent axonemal sheath just below the EC region (Figure 8C, arrowhead). However, this staining may not reveal fine cross bridges of membranous bodies among the spermatids if any such structure exists along the length. In addition, we found an enrichment of DiOC6 staining at the distal ends of spermatids (Figure 8C, arrow), which indicated that growing ends of spermatids contained lipid-rich structures. DiOC6 is a lipid-soluble fluorescent dye that labels all cellular membrane, but it was also shown to preferentially highlight the ER-Golgi–derived membranes in live cells under specific staining conditions (Terasaki *et al*., 1984). The earlier morphological studies also indicated the presence of smooth ER-like membrane lamellae at the distal tips of spermatids (reviewed in Lindsley and Tokuyasu, 1980). Therefore, the EC would be the likely site of the axonemal sheath assembly during spermatid growth,

and this together with the data presented above suggest that DDLC1–DHC–Glued complex would be involved in membrane deposition at the EC region during cell growth.

DISCUSSION

Our results showed that DDLC1 regulates both Dynein and Dynactin activities at the growing ends of spermatids to maintain the spectrin-rich cortical scaffold as well as cell growth at the distal ends, but not the assembly and growth of axoneme. Interestingly, we found that the threshold of DDLC1 actions for the EC assembly and the spermatid growth were different, and together they contribute to the overall growth. All these findings helped to establish that the cell and axoneme growth in the developing spermatids of *Drosophila* are two independent processes, although they occur in synchrony. The cytoplasmic Dynein–Dyanctin complex is implicated to maintain the cell growth in this study, whereas the flagellar axonemes seemed to grow using a hitherto unknown mechanism. Finally, we also showed that partial loss of function alleles of *ddlc1* could be used to study its function in selected cellular processes, because it would affect a subset of its functions in the cell.

Involvement of Dynein–Dynactin complex in spermatid growth is a novel finding of this study. To further explain the implication of our results and to account for the likely role of DDLC1 along with the Dynein–Dynactin complex at the distal ends of spermatids, we propose that a Dynein-Dynactin–dependent retrograde vesicle transport would carry vesicles from the internal membrane store placed at the distal tip of the growing spermatids and deposit them centripetally around the axoneme-mitochondria assembly to form individual axonemal sheath (Figure 9). The membrane deposition sites could be in the EC region at, or, below the spectrin-rich annulus formed around each axoneme complex. Thus, the overall rate of cell growth would be effectively controlled by the rate of vesicular transport, and it should be organized in such a manner that the rate of cell growth would be of the same order to that of the axoneme assembly and growth. This would maintain a synchrony between these two processes. Our study suggests that DDLC1 would regulate such Dynein-Dyanctin–dependent transport. In addition, the Dynein–Dyanctin–DDLC1 complex would also play a role in maintaining the cortical spectrin scaffold in the EC region. Although DLC1/LC8 is found to be an integral component of flagellar axoneme in *Chlamydomonas* (Yang *et al*., 2001), our results indicate that the sperm axoneme assembly is DDLC1 independent.

DDLC1 Regulates Dynein–Dynactin Activity during EC Formation and Maintenance

ECs are derived from fusomes after meiosis and our results show that Ddlc1 plays an important role in maintaining the spectrin cytoskeleton of the EC through the Dynein–Dynactin complex. Fusomes are tubulovesicular structures supported by a spectrin-rich scaffold (de Cuevas *et al*., 1996; de Cuevas and Spradling, 1998) and a microtubule network (Grieder *et al*., 2000). It is known to play an important role in synchronous cell division at the early stages of oogenesis (de Cuevas *et al*., 1996), and *Dhc64C*, as well as the *DLis1* are required to maintain them in the ovary (McGrail and Hays, 1997; Liu *et al*., 1999). Together, these data suggested that a spectrin–microtubule interaction via Dynein–Dynactin complex would play an important role in fusome maintenance. The Dynein–Dynactin complex has also been implicated in maintaining the membranous organelles such the endoplasmic reticulum (ER) and Golgi in cultured cells and *Xenopus* extract (Presley *et al*., 1997; Steffen *et al*., 1997) respectively, which are also supported by a cortical spectrin network. Our results indicate that a similar mechanism is involved in maintaining the spectrin scaffold of the ECs. Because LC8/DLC1 is only known to associate with the IC74 subunit of Dynein motor complex (Lo *et al*., 2001), it could only interact with the $P150^{Glued}$ subunit of Dynactin via IC74 (Vaughan and Vallee, 1995) and thus with the spectrin cytoskeleton of the membrane-bound vesicles (Muresan *et al*., 2001). Therefore, DDLC1 could either have a regulatory role in Dynein–Dynactin interaction, or it could play a critical role in regulating the activities of one or both of them during spermatogenesis.

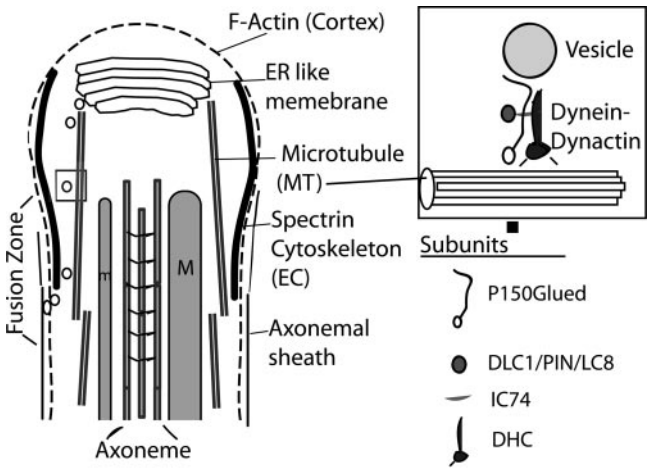

Figure 9. An illustration of the proposed role of cytoplasmic Dynein-Dynactin in the membrane deposition process at the caudal end of growing spermatids. The caudal end of a single elongation stage spermatid is shown in this illustration. The smooth "ER-like membrane" lamellae, the cellular "microtubule (MT)", the major (M) and minor (m) mitochondrial derivatives, "axoneme," the cortical "F-actin" and "spectrin" cytoskeleton assembly of the EC region, and the "axonemal sheath" is indicated with appropriate labels. Growing spermatids remain in syncytium at the distal most end and individual axoneme-mitochondria assembly as shown in this illustration is found to be enveloped in separate axonemal sheath just below the elongation cone region marked by the spectrin rich cytoskeleton. The cytoplasmic Dynactin–Dynactin complex is proposed to transport membrane bound vesicles generated from the ER lamellae to the fusion zone surrounding the axoneme-mitochondria assembly and these vesicles upon fusion would generate the axonemal sheath. The cellular microtubules are likely to play a role in directing the vesicular traffic toward the basal side. The box at the top right corner illustrates how the cellular Dynein–Dynactin subunits could interact with the vesicle and the microtubule. The subunits indicated are the ones tested for their role in spermatid growth in this study. The membrane organization at the caudal most end of spermatid is not shown in this illustration because the ultrastructure of this region is not clearly understood.

DDLC1-dependent Distal End Localization of Dynein–Dynactin Complex and Their Role in Spermatid Growth

In *Chlamydomonas*, the anterograde IFT moves cytoplasmic Dynein to the distal ends of growing flagella, which is required for retrograde IFT as well as the axoneme assembly and flagellar growth (Rosenbaum and Witman, 2002; Qin *et al*., 2004). We found that in *ddlc1* testis, the axonemes are normal, and there was no abnormal accumulation of electron-dense IFT-like particles inside the growing spermatids.

In addition, some recent reports have also established that the anterograde IFT is not involved in spermatogenesis in *Drosophila* (Han *et al*., 2003; Sarpal *et al*., 2003). Therefore, cytoplasmic Dynein-dependent retrograde IFT and flagellar axoneme assembly are unlikely to propel spermatid growth in *Drosophila*. Instead, the DDLC1-dependent Dynein–Dynactin localization at the distal ends of spermatids seems to play an important role in their growth. Similar NUDG-dependent distal end enrichment of Dynein was observed in *Aspergillus* (Beckwith *et al*., 1998; Liu *et al*., 2003), which was essential for hyphal growth, and conventional Kinesin was shown to localize them at the distal ends (Zhang *et al*., 2003). A similar mechanism could be used in spermatids as well.

What would be the role of such distal end enrichment of Dynein in *Drosophila* spermatids? Mutation in rnRacGAP was shown to affect the membrane deposition process involved in spermatid growth, which effectively blocked the cell growth but not that of the axoneme inside (Bergeret *et al*., 2001). In addition, mutations in the fws locus of *Drosophila*, which codes for a protein homologous to the Golgi-associated protein COG5 (Farkas *et al*., 2003) and the Syntaxin-5 (Xue *et al*., 2002), respectively, were also shown to affect spermatid growth. These suggested that fusion of membranous vesicles could play an important role in sperm cell growth. We have also noticed a membranous bulge at the distal end of cysts, and this region is known to contain smooth ER membrane (Lindsley and Tokuyasu, 1980). The cytoplasmic Dynein–Dyanctin complex is known to be involved in vesicular trafficking inside the cell in a variety of different cellular functions, including those involving exocytosis and membrane fusion (Burkhardt *et al*., 1997; Itin *et al*., 1999; Wang *et al*., 2003). Finally, testis-specific knockout of Lis1 is shown to affect acrosomal vesicle fusion and disrupt spermiogenesis (Nayernia *et al*., 2003). In light of all this evidence, it seems that Dynein-Dyanctin–dependent vesicle transport would facilitate the formation of axonemal sheath at the EC region around each growing assembly of axoneme–mitochondria complex (Figure 9). The DDLC1/DHC/Glued-enriched regions at the distal end could mark the starting point for such transport.

Role of Spectrin in Cell Growth at the Distal End

The enrichment of spectrin cytoskeleton at the growing ends of spermatids and its requirement in maintaining cell growth is an interesting finding. Previous studies in cultured PC12 cell showed that a neuron-specific form of spectrin (Calspectin/Fodrin) accumulates at the growing ends of the neurites (Sobue and Kanada, 1989), and the P50 subunit of Dynactin was shown to enrich at the nerve growth cones in mammalian brain (Abe *et al*., 1997). Studies in *Drosophila* have indicated that α- and β-spectrin are essential for maintaining the polarized membrane skeleton assembly in *Drosophila* S2 cells (Dubreuli *et al*., 1997) and the apical assembly of cortical spectrin network in follicle cells (Zarnescu and Thomas, 1999). Furthermore, mutations in the Ddlc1 (*ctp*) locus were reported to cause abnormal targeting of sensory axons in thoracic ganglion (Phillis *et al*., 1996). Interestingly, the sensory axons in *ctp* homozygous adults failed to form proper branches and seemed to grow in altered trajectories. Similar phenotype occurred when a dominant negative Glued gene product was expressed in these neurons (Murphey *et al*., 1999). All these suggest that DDLC1 could also regulate spectrin–Dynactin–Dynein interaction at the growth cones, and this would maintain cell growth.

ACKNOWLEDGMENTS

We thank Prof. D.F. Eberl for a careful reading of the manuscript; Prof. Richard Vallee for kind assistance and support; Profs. R .Dubreueli, R. Scarapulla, D. Ready, and J.M. Scholey for generous supply of antibodies; Prof. William Chia for the fly stocks; and B. Desai for raising DDLC1 antibody and other help. A.G.R. was supported by Kanwal Rekhi Career Development Scholarship, Sarojini Damodaran fellowship, and a travel grant by J. Cell Sci.; K.R. is supported by an intramural grant from the Tata Institute of Fundamental Research, India, DST grant SP/SO/D-76/98 and National Institutes of Health RO3 grant TWO5784.

REFERENCES

Abe, T.K., Tanaka, H., Iwanaga, T., Odani, S., and Kuwano, R. (1997). The presence of the 50-kDa subunit of dynactin complex in the nerve growth cone. Biochem. Biophys. Res. Commun. *233*, 295–299.

Arama, E., Agapite, J., and Steller, H. (2003). Caspase activity and a specific cytochrome C are required for sperm differentiation in *Drosophila*. Dev. Cell. *4*, 687–697.

Beckwith, S.M., Roghi, C.H., Liu, B., and Ronald Morris, N. (1998). The "8-kD"cytoplasmic dynein light chain is required for nuclear migration and for dynein heavy chain localization in *Aspergillus nidulans*. J. Cell Biol. *143*, 1239–1247.

Bergeret, E., Pignot-Paintrand, I., Guichard, A., Raymond, K., Fauvarque, M.O., Cazemajor, M, and Griffin-Shea, R. (2001). RotundRacGAP functions with Ras during spermatogenesis and retinal differentiation in *Drosophila melanogaster*. Mol. Cell. Biol. *21*, 6280–6291.

Burkhardt, J.K., Echeverri, C.J., Nilsson, T., and Vallee, R.B. (1997). Overexpression of the dynamitin (p50) subunit of the dynactin complex disrupts dynein-dependent maintenance of membrane organelle distribution. J. Cell Biol. *139*, 469–484.

Chu, D.T.W., and Klymkowsky, M.W. (1989). The appearance of acetylated a-tubulin during early development and cellular differentiation in *Xenopus*. Dev. Biol. *136*, 104–117.

de Cuevas, M., Lee, J.K., and Spradling, A.C. (1996). Alpha-spectrin is required for germline cell division and differentiation in the *Drosophila* ovary. Development *122*, 3959–3968.

de Cuevas, M., and Spradling, A.C. (1998). Morphogenesis of the Drosophila fusome and its implications for oocyte specification. Development *125*, 2781–2789.

Daniels, S.B., Mccarron, M., Love, C., and Chovnik, A. (1985). Dysgenesis-induced instability of rosy locus transformation in *Drosophila melanogaster*: analysis of excision events and the selective recovery of control element deletions. Genetics *109*, 95–117.

Delattre, M., Anxolabehere, D., and Coen, D. (1995). Prevalence of localized rearrangements *vs.* transpositions among events induced by *Drosophila P* element transposase on a *P* transgene. Genetics *141*, 1407–1424.

Dick, T., Ray, K., Salz, H.K., and Chia, W. (1996). Cytoplasmic dynein (ddlc1) mutations cause morphogenetic defects and apoptotic cell death in *Drosophila* melanogaster. Mol. Cell. Biol. *16*, 1966–1977.

Dubreuil, R., Byers, T.J., Branton, D., Goldstein, L.S.B., and Kiehart, D.P. (1987). *Drosophila* spectrin I. characterization of the purified protein. J. Cell Biol. *105*, 2095–2102.

Dubreuil, R.R., Maddux, P.B., Grushko, T.A., and MacVicar, G.R. (1997). Segregation of two spectrin isoforms, polarized membrane-binding sites direct polarized membrane skeleton assembly. Mol. Biol. Cell *8*, 1933–1942.

Epstein, E., Sela-Brown, A., Ringel, I., Kilav, R., King, S.M., Benashski, S.E., Yisraeli, J.K., Silver, J., and Naveh-Many, T. (2000). Dynein light chain binding to a 3′-untranslated sequence mediates parathyroid hormone mRNA association with microtubules. J. Clin. Investig. *105*, 505–512.

Fabrizio, J.J., Hime, G., Lemmon, S.K., and Bazinet, C. (1998). Genetic dissection of sperm individualization in *Drosophila melanogaster*. Development *125*, 1833–1843.

Fan, S.S., and Ready, D.F. (1997). Glued participates in distinct microtubule-based activities in *Drosophila* eye development. Development *124*, 1497–1507.

Farkas, R.M., Giansanti, M.G., Gatti, M., and Fuller, M.T. (2003). The *Drosophila* Cog5 homologue is required for cytokinesis, cell elongation, and assembly of specialized Golgi architecture during spermatogenesis. Mol. Biol. Cell *14*, 190–200.

Fuller, M.T. (1993). Spermatogenesis. In: The Development of *Drosophila melanogaster*, ed. M. Bate and A.M. Arias, Cold Spring Harbor, NY: Cold Spring Harbor Press, 71–147.

Gepner, J., Li, M., Ludmann, S., Kortas, C., Boylan, K., Iyadurai, S.J., McGrail, M., and Hays, T.S. (1996). Cytoplasmic dynein function is essential in Drosophila melanogaster. Genetics *142*, 865–878.

Grieder, N.C., de Cuevas, M., and Spradling, A.C. (2000). The fusome organizes the microtubule network during oocyte differentiation in *Drosophila*. Development *127*, 4253–4264.

Han, Y.G., Kwok, B.H., and Kernan, M. (2003). Intraflagellar transport is required in *Drosophila* to differentiate sensory cilia but not sperm. Curr. Biol. *13*, 1679–1686.

Harlow, E., and Lane, D. (1988). Antibodies: A Laboratory Manual, Cold Spring Harbor, NY: Cold Spring Harbor Laboratory Press.

Herzig, R.P., Andersson, U., and Scarpulla, R.C. (2000). Dynein light chain interacts with NRF-1 and EWG, structurally and functionally related transcription factors from humans and *Drosophila*. J. Cell Sci. *113*, 4263–4273.

Hicks, J.L., Deng, W.M., Rogat, A.D., Miller, K.G., and Bownes, M. (1999) Class VI unconventional myosin is required for spermatogenesis in *Drosophila*. Mol. Biol. Cell *10*, 4341–4353.

Hime, G.R., Brill, J.A., and Fuller, M.T. (1996). Assembly of ring canals in the male germ line from structural components of the contractile ring. J. Cell Sci. *109*, 2779–2788.

Itin, C., Ulitzur, N., Muhlbauer, B., and Pfeffer, S.R. (1999). Mapmodulin, cytoplasmic dynein, and microtubules enhance the transport of mannose 6-phosphate receptors from endosomes to the trans-Golgi network. Mol. Biol. Cell *10*, 2191–2197.

Jaffrey, S.R., and Snyder, S.H. (1996). PIN: an associated protein inhibitor of neuronal nitric oxide synthase. Science *274*, 774–777.

King, S.M., Barbarese, E., Dillman, J.F.III., Patel-King, R.S., Carson, J.H., and Pfister, K.K. (1996). Brain cytoplasmic and flagellar outer arm dyneins share a highly conserved Mr 8,000 light chain. J. Biol. Chem. *271*, 19358–19366.

King, S.M., and Patel-King, R.S. (1995). The M(r) = 8,000 and 11,000 outer arm dynein light chains from Chlamydomonas flagella have cytoplasmic homologues. J. Biol. Chem. *270*, 11445–11452.

Kozminski, K.G., Beech, P.L., and Rosenbaum, J.L. (1995). The *Chlamydomonas* kinesin-like protein FLA10 is involved in motility associated with the flagellar membrane. J. Cell Biol. *131*, 1517–1527.

Liang, J., Jaffrey, S.R., Guo, W., Snyder, S.H., and Clardy, J. (1999). Structure of the PIN/LC8 dimer with a bound peptide. Nat. Struct. Biol. *6*, 735–740.

Liu, B., Xiang, X., and Lee, Y.R. (2003). The requirement of the LC8 dynein light chain for nuclear migration and septum positioning is temperature dependent in *Aspergillus nidulans*. Mol. Microbiol. *47*, 291–301.

Liu, Z., Xie, T., and Steward, R. (1999). Lis1, the *Drosophila* homolog of a human lissencephaly disease gene, is required for germline cell division and oocyte differentiation. Development *126*, 4477–4488.

Lindsley, D.L., and Tokuyasu, K.T. (1980). Spermatogenesis, Chapter 32, Vol 2d, The Genetics and Biology of *Drosophila*, ed. Ashburner M and Write TRF, Oxford: Academic Press, 226–287.

Lo, K.W., Naisbitt, S., Fan, J.S., Sheng, M., and Zhang, M. (2001). The 8-kDa dynein light chain binds to its targets via a conserved (K/R)XTQT motif. J. Biol. Chem. *276*, 14059–14066.

Makokha, M., Hare, M., Li, M., Hays, T., and Barbar, E. (2002). Interactions of cytoplasmic dynein light chains Tctex-1 and LC8 with the intermediate chain IC74. Biochemistry *41*, 4302–4311.

McGrail, M., and Hays, T.S. (1997). The microtubule motor cytoplasmic dynein is required for spindle orientation during germline cell divisions and oocyte differentiation in *Drosophila*. Development *124*, 2409–2419.

Muresan, V., Stankewich, M.C., Steffen, W., Morrow, J.S., Holzbaur, E.L., and Schnapp, B.J. (2001). Dynactin-dependent, dynein-driven vesicle transport in the absence of membrane proteins, a role for spectrin and acidic phospholipids. Mol. Cell. *7*, 173–183.

Murphey, R.K., Caruccio, P.C., Getzinger, M., Westgate, P.J., and Phillis, R.W. (1999). Dynein-dynactin function and sensory axon growth during Drosophila metamorphosis: a role for retrograde motors. Dev. Biol. *209*, 86–97.

Nayernia, K., Vauti, F., Meinhardt, A., Cadenas, C., Schweyer, S., Meyer, B.I., Schwandt, I., Chowdhury, K., Engel, W., and Arnold, H.H. (2003) Inactivation of a testis-specific Lis1 transcript in mice prevents spermatid differentiation and causes male infertility. J. Biol. Chem. *278*, 48377–48385.

Noguchi, T., and Miller, K.G. (2003). A role for actin dynamics in individualization during spermatogenesis in *Drosophila melanogaster*. Development *130*, 1805–1816.

Naisbitt, S., Valtschanoff, J., Allison, D.W., Sala, C., Kim, E., Craig, A.M., Weinberg, R.J., and Sheng, M. (2000). Interaction of the postsynaptic density-95/guanylate kinase domain-associated protein complex with a light chain of myosin-V and dynein. J. Neurosci. *20*, 4524–4534.

Pazour, G.J., Wilkerson, C.G., and Witman, G.B. (1998). A dynein light chain is essential for the retrograde particle movement of intraflagellar transport (IFT). J. Cell Biol. *141*, 979–992.

Phillis, R., Statton, D., Caruccio, P., and Murphey, R.K. (1996). Mutations in the 8 kDa dynein light chain gene disrupt sensory axon projections in the Drosophila imaginal CNS. Development. *122*, 2955–63.

Presley, J.F., Cole, N.B., Schroer, T.A., Hirschberg, K., Zaal, K.J., and Lippincott-Schwartz, J. (1997). ER-to-Golgi transport visualized in living cells. Nature. *389*, 81–85.

Qin, H., Diener, D.R., Geimer, S., Cole, D.G., and Rosenbaum, J.L. (2004). Intraflagellar transport (IFT) cargo: IFT transports flagellar precursors to the tip and turnover products to the cell body. J. Cell Biol. *164*, 255–266.

Qin, H., Rosenbaum, J.L., and Barr, M.M. (2001). An autosomal recessive polycystic kidney disease gene homolog is involved in intraflagellar transport in C. elegans ciliated sensory neurons. Curr. Biol. *11*, 457–461.

Rogat, A.D., and Miller, K.G. (2002). A role for myosin VI in actin dynamics at sites of membrane remodeling during *Drosophila* spermatogenesis. J. Cell Sci. *115*, 4855–4865.

Rorth, P. (1998). Gal4 in the *Drosophila* female germline. Mech. Dev. *78*, 113–118.

Rosenbaum, J.L., and Witman, G.B. (2002). Intraflagellar transport. Nat. Rev. Mol. Cell. Biol. *3*, 813–825.

Raux, H., Flamand, A., and Blondel, D. (2000). Interaction of the rabies virus P protein with the LC8 dynein light chain. J. Virol. *74*, 10212–10216.

Rodriguez-Crespo, I., Yelamos, B., Roncal, F., Albar, J.P., Ortiz de Montellano, P.R., and Gavilanes, F. (2001). Identification of novel cellular proteins that bind to the LC8 dynein light chain using a pepscan technique. FEBS Lett. *503*, 135–141.

Sarpal, R., Todi, S.V., Sivan-Loukianova, E., Shirolikar, S., Subramanian, N., Raff, E.C., Erickson, J.W., Ray, K., and Eberl, D.F. (2003). *Drosophila* kinesin associated protein (DmKap) interacts with the kinesin II motor subunit Klp64D to assemble chordotonal sensory cilia but not sperm tails. Curr. Biol. *13*, 1687–1696.

Schnorrer, F., Bohmann, and, K., Nusslein-Volhard, C. (2000). The molecular motor dynein is involved in targeting swallow and bicoid RNA to the anterior pole of Drosophila oocytes. Nat. Cell Biol. *2*, 185–90.

Sharp, D.J., Brown, H.M., Kwon, M., Rogers, G.C., Holland, G., and Scholey, J.M. (2000). Functional coordination of three mitotic motors in *Drosophila* embryos. Mol. Biol. Cell *11*, 241–253.

Signor, D., Wedaman, K.P., Orozco, J.T., Dwyer, N.D., Bargmann, C.I., Rose, L.S., and Scholey, J.M. (1999). Role of a class DHC1b dynein in retrograde transport of IFT motors and IFT raft particles along cilia, but not dendrites, in chemosensory neurons of living *Caenorhabditis elegans*. J. Cell Biol. *147*, 519–530.

Spradling, A.C., Stern, D., Kiss, I., Roote, J., and Laverty, T. (1995). Gene disruptions using *P* transposable elements: an integral component of the *Drosophila* genome project. Proc. Natl. Acad. Sci. USA *92*, 10824–10830.

Spradling, A.C., Stern, D., Beaton, A., Rhem, E.J., and Laverty, T. (1999). The BDGP gene disruption project: single *P* element insertions mutating 25% of vital *Drosophila* genes. Genetics *153*, 135–177.

Sobue, K., and Kanda, K. (1989). Alpha-actinins, calspectin (brain spectrin or fodrin), and actin participate in adhesion and movement of growth cones. Neuron *3*, 311–319.

Steffen, W., Karki, S., Vaughan, K.T., Vallee, R.B., Holzbaur, E.L., Weiss, D.G., and Kuznetsov, S.A. (1997). The involvement of the intermediate chain of cytoplasmic dynein in binding the motor complex to membranous organelles of *Xenopus* oocytes. Mol. Biol. Cell *8*, 2077–2088.

Taulman, P.D., Haycraft, C.J., Balkovetz, D.F., and Yoder, B.K. (2001). Polaris, a protein involved in left-right axis patterning, localizes to basal bodies and cilia. Mol. Biol. Cell *12*, 589–599.

Terasaki, M., Song, J., Wong, J.R., Weiss, M.J., and Chen, L.B. (1984). Localization of endoplasmic reticulum in living and glutaraldehyde-fixed cells with fluorescent dyes. Cell. *38*, 101–8.

Timakov, B., Liu, X., Turgut, I., and Zhang, P. (2002). Timing and targeting of P-element local transposition in the male germline cells of *Drosophila melanogaster*. Genetics. *160*, 1011–1022.

Tochio, H., Ohki, S., Zhang, Q., Li, M., and Zhang, M. (1998). Solution structure of a protein inhibitor of neuronal nitric oxide synthase. Nat. Struct. Biol. *5*, 965–969.

Van Doren, M., Williamson, A.L., and Lehmann, R. (1998). Regulation of zygotic gene expression in *Drosophila* primordial germ cells. Curr. Biol. *8*, 243–246.

Vaughan, K.T., and Vallee, R.B. (1995). Cytoplasmic dynein binds dynactin through a direct interaction between the intermediate chains and p150Glued. J. Cell Biol. *131*, 1507–16.

Voelker, R.A., Greenleaf, A.L., Gyurkovics, H., Wisly, G.B., and Huang S. M.,. (1984). Frequent imprecise excision among reversions of a *P* element-caused lethal mutations in *Drosophila*. Genetics *107*, 279–294.

Wang, Y., *et al*. (2003). Cytoplasmic dynein participates in apically targeted stimulated secretory traffic in primary rabbit lacrimal acinar epithelial cells. J. Cell Sci. *116*, 2051–2065.

Wodarz, A., Hinz, U., Engelbert, M., and Knust, E. (1995). Expression of crumbs confers apical character on plasma membrane domains of ectodermal epithelia of *Drosophila*. Cell *82*, 67–76.

Xu, H., Brill, J.A., Hsien, J., McBride, R., Boulianne, G.L., and Trimble, W.S. (2002). Syntaxin 5 is required for cytokinesis and spermatid differentiation in *Drosophila*. Dev. Biol. *251*, 294–306.

Yang, P., Diener, D.R., Rosenbaum, J.L., and Sale, W.S. (2001). Localization of calmodulin and dynein light chain LC8 in flagellar radial spokes. J. Cell Biol. *153*, 1315–1326.

Zarnescu, D.C., and Thomas, G.H. (1999). Apical spectrin is essential for epithelial morphogenesis but not apicobasal polarity in *Drosophila*. J. Cell Biol. *146*, 1075–1086.

Zhang, J., Li, S., Fischer, R., and Xiang, X. (2003). Accumulation of cytoplasmic dynein and dynactin at microtubule plus ends in *Aspergillus nudilans* is kinesin dependent. Mol. Biol. Cell *14*, 1479–1488.

Zhang, P., and Spradling, A.C. (1993). Efficient and dispersed local *P*-element transposition from *Drosophila* females. Genetics. *133*, 361–373.